# Microwave conductivity of *d*-wave superconductors with extended impurities

Tamara S. Nunner and P. J. Hirschfeld
*Department of Physics, University of Florida, Gainesville, Florida 32611-8440, USA*
(Received 11 November 2004; published 8 July 2005)

We investigate the influence of extended scatterers on the finite temperature and finite frequency microwave conductivity of *d*-wave superconductors. For this purpose we generalize a previous treatment by Durst and Lee, which is based on a nodal approximation of the quasiparticle excitations and scattering processes, and apply it to the analysis of experimental spectra of YBCO-123 and BSCCO-2212. For YBCO, we find that accounting for a slight spatial extension of the strong scattering in-plane defects improves the fit of the low temperature microwave conductivity to experiment. With respect to BSCCO we conclude that it is necessary to include a large concentration of weak-to-intermediate strength extended scatterers, which we attribute to the out-of plane disorder introduced by doping. These findings for BSCCO are consistent with similar analyses of the normal state ARPES spectra and of STM spectra in the superconducting state, where an enhanced forward scattering has been inferred as well.

DOI: 10.1103/PhysRevB.72.014514 PACS number(s): 74.72.−h, 74.25.Fy, 74.25.Nf

## I. INTRODUCTION

Early in the debate over the symmetry of the superconducting order in the cuprates, a rather convincing picture of the microwave properties of the YBCO-123 system was put forward by Bonn *et al.*,[1] and later placed on a microscopic foundation.[2–4] Crucial to this interpretation is the observed collapse of the *d*-wave nodal quasiparticle scattering rate as the system becomes superconducting,[5–7] leading to a dramatic rise in the conductivity with decreasing temperature. This rise is cut off when the inelastic mean free path becomes comparable to the elastic one, and the conductivity subsequently decreases because of the vanishing nodal carrier density as temperature tends to zero. One consequence of this picture is that the resulting conductivity peak should be suppressed and occur at higher temperatures in dirtier samples. In addition, the conductivity should approach the universal value $\sigma_0 = e^2 v_f/(\hbar \pi^2 v_2)$ for zero temperature and zero frequency as predicted by P. A. Lee[8] for the case of isotropic scatterers, where $v_F$ is the Fermi velocity and $v_2$ the gap velocity at the node.

If one extracts $v_F/v_2$ from thermal conductivity[9] or angle resolved photoemission (ARPES) measurements,[10] one finds that the universal value for both BSCCO and YBCO crystals should be about $\sigma_0 = 5 \times 10^5\ \Omega^{-1}\ \mathrm{m}^{-1}$. In YBCO, the residual value of the conductivity for $\omega, T \to 0$ is difficult to determine, but appears to be approaching $3–4\sigma_0$ in the best crystals.[11] The peak in the conductivity occurs around 25 K with an amplitude of approximately $100\sigma_0$ for the lowest frequency measured. In BSCCO, the peak is located around 20 K, but is only about 20% higher than the apparent residual value[12] of $8–10\sigma_0$. Virtually no frequency dependence is seen in the measured microwave frequency range,[12] suggesting a very dirty material, in apparent contradiction—within the "standard" scenario—with the low-temperature peak position. The long-standing puzzle of the low temperature microwave peak together with indications of dirty limit behavior have been analyzed as evidence for absorption into a collective mode off resonance at low frequencies,[13] as well as a consequence of nanoscale inhomogeneity.[14]

In this work we argue that the temperature dependence of the conductivity can be more naturally understood in terms of the effect of extended scatterers present in the BSCCO crystal. Current generation crystals are made typically with excess Bi, deficiencies of Sr and Ca, and excess O content; cation substitution is thought to occur frequently. Some aspects of this defect distribution have been discussed recently by Eisaki *et al.*[15] The net result of these defects is not only to dope the nominally stoichiometric BSCCO crystal (pure BSCCO would be an insulator), but to provide a relatively slowly varying potential landscape for quasiparticles moving in the $CuO_2$ planes. The effect of these extended scatterers with respect to the normal state has recently been discussed by Abrahams and Varma[16] and it has been pointed out by Zhu *et al.*[17] that the broad momentum space peaks observed in Fourier transform STM studies of BSCCO[18–20] can only be explained by potential scatterers with finite range. In a further application of this notion to ARPES, Zhu *et al.*[21] showed that a large concentration of impurities with potentials peaked in the forward direction could be present without substantially broadening quasiparticle states except near the node. Since the microwave conductivity is dominated by nodal quasiparticles, it is clearly important to ask what the effects of extended or forward scatterers are in this case.

Since the work of Durst and Lee,[22] we know that the residual conductivity in the presence of extended scatterers can be much larger than the "universal" value $\sigma_0$. This might account for the large value of the microwave conductivity observed in the BSCCO-2212 system at low temperatures. To make this case, however, one needs to examine the influence of a finite scattering range at finite temperatures and frequencies. We have therefore generalized the analysis of Durst and Lee in this way and applied this treatment to the analysis of experiments on YBCO and BSCCO.

The outline of the paper is as follows. In Sec. II, we describe the model and derive expressions for the self-energy and vertex function for extended scatterers. Our approach, which is based on an extension of the work by Durst and Lee,[22] aims at treating scattering potentials with an extension

 

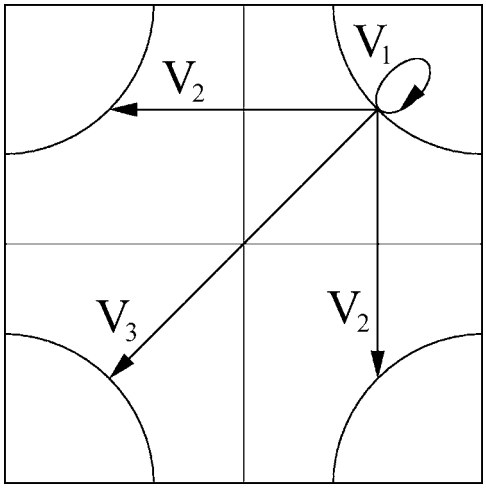


FIG. 1. For low temperatures and low frequencies the momentum transfer between quasiparticles is basically limited to the four wave vectors connecting the nodes of a *d*-wave superconductor. Therefore the momentum dependent impurity potential $V(k)$ can be represented by the values at the respective wave vectors, i.e., by three parameters $V_1$, $V_2$, and $V_3$.

of a few lattice spacings at maximum and is therefore in the opposite limit from semiclassical calculations where the impurity potentials extend over a few coherence lengths.[23,24] In Sec. III we apply our treatment to the microwave conductivity of YBCO. We show that the consideration of slightly extended instead of pointlike strong potential scatterers improves the agreement with the experimental spectra. In Sec. IV we address the microwave conductivity of BSSCO and demonstrate that it is necessary to include a large concentration of weak extended scatterers in order to explain the experimental spectra. A good fit is obtained based on a realistic disorder model for BSCCO which contains weak extended scatterers in addition to strong pointlike in-plane defects which are responsible for the unitary scattering resonances observed by STM. Finally, in Sec. IV, we present our conclusions.

## II. TREATMENT OF EXTENDED SCATTERERS

For low temperatures and low frequencies the quasiparticle dispersion of a *d*-wave superconductor can be linearized around the nodes. The resulting quasiparticle spectrum has the form of a Dirac cone, whose anisotropy is determined by the ratio $v_f/v_2$ of the Fermi velocity $v_f=\partial\epsilon_k/\partial k=2\sqrt{2}t$ and the gap velocity $v_2=\partial\Delta_k/\partial k=\Delta_0/\sqrt{2}$, where $t$ is the nearest neighbor hopping parameter and $\Delta_0$ is the maximum gap value and we have set $a=\hbar=1$. At low temperatures and frequencies, quasiparticle excitations are restricted to small regions around the nodes. Therefore momentum transfer between quasiparticles is limited to four wave vectors which connect the four nodes and include intranode and internode scattering processes (see Fig. 1). Consequently a momentum dependent impurity potential $V_{kk'}$ can be represented by three parameters $V_1$, $V_2$, and $V_3$ which correspond to the respective momentum transfers. For zero temperature and zero frequency when the nodes reduce to points this nodal approximation for the impurity potential can reproduce any impurity potential. For finite temperatures and frequencies, however, this approximation poses a limitation on the forward scattering character of the impurity potential because it assumes constant potential within one node, i.e., for all momenta in a Brillouin zone quadrant around a particular node. Although the strict forward scattering limit can therefore not be reached for finite temperatures and frequencies, this approximation is still appropriate to treat intermediate range scatterers as considered here.

Based on these approximations and treating impurity scattering in *T*-matrix approximation, an expression for the microwave conductivity has been derived by Durst and Lee.[22] They found that vertex corrections, which arise from the momentum dependence of the impurity potential, induce a dependence of the zero-temperature and zero-frequency limit of the conductivity on the impurity potential and the impurity concentration. Contrary to the case of pointlike scatterers, no universal value of the electrical conductivity exists therefore in case of extended scatterers. Durst and Lee, however, did not further explore the frequency and temperature dependence of the microwave conductivity. Here, we generalize their approach to finite frequencies and temperatures and consider the effect of combining different types of scatterers.

### A. Self-energy

Before proceeding to two-particle quantities like the microwave conductivity, it is instructive to focus first on single-particle properties like the single-particle self-energy. Using the Nambu notation, the disorder-averaged single-particle self-energy in a superconductor can be decomposed as

$$\tilde{\Sigma}(k,\omega)=\sum_{\alpha}\Sigma_{\alpha}(k,\omega)\tilde{\tau}_{\alpha}, \tag{1}$$

where $\tilde{\tau}_{\alpha}$ are the Pauli matrices and $\tilde{\tau}_0$ is the unit matrix. Treating impurity scattering in *T*-matrix approximation gives rise to the following self-energy:

$$\tilde{\Sigma}(k,\omega)=n_i\tilde{T}_{kk}(\omega), \tag{2}$$

where $n_i$ is the impurity concentration and $T_{kk}(\omega)$ is the diagonal element of the *T*-matrix,

$$\tilde{T}_{kk'}(\omega)=V_{kk'}\tilde{\tau}_3+\sum_{k''}V_{kk''}\tilde{\tau}_3\tilde{G}(k'',\omega)\tilde{T}_{k''k'}(\omega). \tag{3}$$

The self-energy $\tilde{\Sigma}(k,\omega)$ must be solved self-consistently in combination with the single-particle Green's function,

$$\tilde{G}(k,\omega)^{-1}=\tilde{G}_0(k,\omega)^{-1}-\tilde{\Sigma}(k,\omega), \tag{4}$$

where the unperturbed Green's function is given as

$$\tilde{G}_0(k,\omega)=\frac{\omega\tilde{\tau}_0+\Delta_k\tilde{\tau}_1+\epsilon_k\tilde{\tau}_3}{\omega^2-\epsilon_k^2-\Delta_k^2}. \tag{5}$$

Following the approach of Durst and Lee,[22] we reduce the impurity scattering potential to the four wave vectors connecting the nodes, i.e., $V_{kk'}$ is replaced by a $4\times4$-matrix in nodal space,

$$V_{kk'} \to \underline{V} = \begin{pmatrix} V_1 & V_2 & V_3 & V_2 \\ V_2 & V_1 & V_2 & V_3 \\ V_3 & V_2 & V_1 & V_2 \\ V_2 & V_3 & V_2 & V_1 \end{pmatrix}, \tag{6}$$

where $V_1$, $V_2$, and $V_3$ are the values of the impurity potential at the wave vectors connecting the nodes, see Fig. 1.

Using this simplification, the impurity potential can be pulled out of the integral and the $T$-matrix becomes a $4\times4$-matrix in nodal space

$$\tilde{T}_{jj'}(\omega) = V_{jj'}\tilde{\tau}_3 + \tilde{I}_G(\omega)\tilde{\tau}_3 \sum_{j''} V_{jj''}\tilde{T}_{j''j'}(\omega), \tag{7}$$

where $\tilde{I}_G(\omega)$ is the integral of the single-particle Green's function over one-quarter of the Brillouin zone,

$$\tilde{I}_G(\omega) = \int_0^\pi \int_0^\pi \frac{d^2k}{(2\pi)^2}\tilde{G}(k,\omega) = g_0(\omega)\tilde{\tau}_0 + g_3(\omega)\tilde{\tau}_3. \tag{8}$$

This allows for an analytical solution[22] of the $T$-matrix,

$$\tilde{T}_{jj'} = T^3_{jj'}\tilde{\tau}_3 + T^0_{jj'}\tilde{\tau}_0 \tag{9}$$

with

$$T^3_{jj'} = \left(\frac{[1-g_3(\omega)\underline{V}]\underline{V}}{[1-g_3(\omega)\underline{V}]^2 - g_0(\omega)^2\underline{V}^2}\right)_{jj'},$$
$$T^0_{jj'} = \left(\frac{g_0(\omega)\underline{V}^2}{[1-g_3(\omega)\underline{V}]^2 - g_0(\omega)^2\underline{V}^2}\right)_{jj'}, \tag{10}$$

where the denominators must be calculated as inverse matrices in nodal space. This gives for the $\Sigma_0$ component of the self-energy,

$$\Sigma_0(\omega) = \frac{n_i}{4}\left(\frac{2g_0(\omega)(V_1-V_3)^2}{[1-g_3(\omega)(V_1-V_3)]^2-[g_0(\omega)(V_1-V_3)]^2} + \frac{g_0(\omega)(V_1-2V_2+V_3)^2}{[1-g_3(\omega)(V_1-2V_2+V_3)]^2-[g_0(\omega)(V_1-2V_2+V_3)]^2} + \frac{g_0(\omega)(V_1+2V_2+V_3)^2}{[1-g_3(\omega)(V_1+2V_2+V_3)]^2-[g_0(\omega)(V_1+2V_2+V_3)]^2}\right). \tag{11}$$

For an isotropic impurity potential, i.e., $V_1=V_2=V_3=V$ this expression simplifies to

$$\Sigma_0^{\rm iso}(V,\omega) = \frac{n_i 4 g_0(\omega)V^2}{[1-4g_3(\omega)V]^2-[4g_0(\omega)V]^2}, \tag{12}$$

which implies that the self-energy in Eq. (11) can be decomposed into a sum of self-energies corresponding to three different isotropic impurity potentials,

$$\Sigma_0(\omega) = \Sigma_0^{\rm iso}\left(\tfrac{1}{4}(V_1+2V_2+V_3),\omega\right) + \Sigma_0^{\rm iso}\left(\tfrac{1}{4}(V_1-2V_2+V_3),\omega\right) + 2\Sigma_0^{\rm iso}\left(\tfrac{1}{4}(V_1-V_3),\omega\right). \tag{13}$$

Consequently, the self-energy for an anisotropic impurity potential in the nodal approximation contains up to three resonances corresponding to the different impurity strengths $V=(V_1+2V_2+V_3)/4$, $V=(V_1-2V_2+V_3)/4$, and $V=(V_1-V_3)/4$, see Fig. 2.

Note that $\Sigma_1$ vanishes in our approach and $\Sigma_3$ plays no important role. While $\Sigma_3$ itself is not necessarily always small (see inset of Fig. 2), its contribution to the single-particle scattering rate $\tau^{-1}$ vanishes at the node,

$$\tau^{-1}(\omega,k) = -2\left(\mathrm{Im}\,\Sigma_0(\omega) + \frac{\xi_k}{\omega}\mathrm{Im}\,\Sigma_3(\omega) + \frac{\Delta_k}{\omega}\mathrm{Im}\,\Sigma_1(\omega)\right) \to -2\,\mathrm{Im}\,\Sigma_0(\omega) \quad \text{for } k = k_{\rm node}, \tag{14}$$

and its contribution to the conductivity is small because it is invariably suppressed by particle-hole asymmetry factors. We nevertheless include the effect of $\Sigma_3$ in numerical evaluations for completeness.

If the scattering strength of the impurities is weak, they can be treated within Born approximation and the self-energy of an extended weak impurity becomes

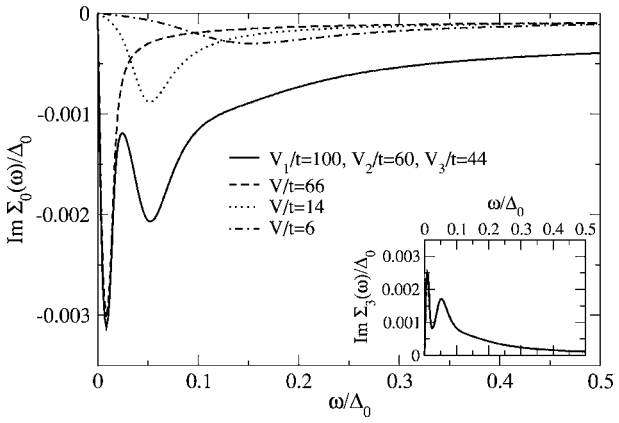


FIG. 2. Imaginary part of the self-consistently calculated self-energy $\Sigma_0(\omega)$ for an anisotropic impurity potential characterized by the three parameters $V_1/t=100$, $V_2/t=60$, and $V_3/t=44$ (solid line). The positions of the resonances coincide with the resonances of the self-energies for isotropic impurity potentials $V/t=66$, $V/t=14$, and $V/t=6$. Here $\Delta_0/t=0.29$ and $n_i=0.00002$ have been used. The inset shows the imaginary part of $\Sigma_3(\omega)$ for the same anisotropic impurity potential $V_1/t=100$, $V_2/t=60$, and $V_3/t=44$.

$$\Sigma_0(\omega) = -n_i(V_1^2 + 2V_2^2 + V_3^2)g_0(\omega), \tag{15}$$

i.e., the self-energy for an anisotropic impurity potential is identical to the self-energy for an isotropic impurity potential with $V=\sqrt{V_1^2+2V_2^2+V_3^2}$.

### B. Microwave conductivity

In linear response the electrical conductivity is given as

$$\sigma(\Omega,T) = -\frac{\mathrm{Im}\,\Pi_{\mathrm{ret}}(\Omega,T)}{\Omega}, \tag{16}$$

where $\Pi_{\mathrm{ret}}(\Omega,T)$ is the retarded current-current correlation function, which can be obtained by analytical continuation from

$$\Pi(i\Omega) = \frac{e^2 v_f^2}{\beta}\sum_{i\omega,k}\mathrm{Tr}[\tilde{G}(k,i\omega)\tilde{G}(k,i\omega+i\Omega)\tilde{\Gamma}(k,i\omega+i\Omega)], \tag{17}$$

where $\tilde{\Gamma}(k,i\omega+i\Omega)$ is the vertex function, which for a $d$-wave superconductor arises entirely from the momentum dependence of the impurity potential[25] and will be calculated here as the sum of ladder diagrams.

Summing up all ladder diagrams one arrives at the following expression for the current-current correlation function:

$$\Pi(i\Omega) = \frac{e^2 v_f}{\pi v_2}\frac{1}{\beta}\sum_{i\omega} J(i\omega,i\Omega) \tag{18}$$

with

$$J = \frac{I_0^0 + \gamma_A(I_0^0 I_3^3 + I_0^3 I_3^0)}{[1-(\gamma_A I_0^0 + \gamma_B I_3^0)][1-(\gamma_B I_0^3 + \gamma_A I_3^3)] - (\gamma_A I_0^3 + \gamma_B I_3^3)(\gamma_B I_0^0 + \gamma_A I_3^0)}, \tag{19}$$

where the frequency indices have been omitted for simplicity. This expression for $J$ is similar to the one derived by Durst and Lee[22] but contains additional terms arising from the finite $\Sigma_3$ component of the single-particle self-energy. The momentum integrated particle-hole bubbles $I_\alpha^\beta(i\omega,i\Omega)$ in Eq. (19) are

$$\begin{aligned} I_0^0\tilde{\tau}_0 + I_0^3\tilde{\tau}_3 &= \int_0^\pi\int_0^\pi \frac{d^2k}{(2\pi)^2}\tilde{G}(k,i\omega)\tilde{G}(k,i\omega+i\Omega), \\ I_3^0\tilde{\tau}_0 + I_3^3\tilde{\tau}_3 &= \int_0^\pi\int_0^\pi \frac{d^2k}{(2\pi)^2}\tilde{G}(k,i\omega)\tilde{\tau}_3\tilde{G}(k,i\omega+i\Omega), \end{aligned} \tag{20}$$

and the vertex functions $\gamma_A, \gamma_B$ are given as

$$\begin{aligned} \gamma_A(i\omega,i\Omega) = \frac{n_i}{4\pi v_f v_2}[&T_{11}^0(i\omega)T_{11}^0(i\omega+i\Omega) \\ &+ T_{11}^3(i\omega)T_{11}^3(i\omega+i\Omega) - T_{13}^0(i\omega)T_{13}^0(i\omega+i\Omega) \\ &- T_{13}^3(i\omega)T_{13}^3(i\omega+i\Omega)], \end{aligned} \tag{21}$$

$$\begin{aligned} \gamma_B(i\omega,i\Omega) = \frac{n_i}{4\pi v_f v_2}[&T_{11}^0(i\omega)T_{11}^3(i\omega+i\Omega) \\ &+ T_{11}^3(i\omega)T_{11}^0(i\omega+i\Omega) - T_{13}^0(i\omega)T_{13}^3(i\omega+i\Omega) \\ &- T_{13}^3(i\omega)T_{13}^0(i\omega+i\Omega)]. \end{aligned}$$

After analytical continuation the microwave conductivity can be expressed as[22]

$$\begin{aligned} \sigma(\Omega) = \frac{e^2 v_f}{2\pi^2 v_2}\int d\omega \frac{n_F(\omega)-n_F(\omega+\Omega)}{\Omega} \\ \times[\mathrm{Re}\,J(\omega-i\delta,\omega+\Omega+i\delta) \\ - \mathrm{Re}\,J(\omega+i\delta,\omega+\Omega+i\delta)]. \end{aligned} \tag{22}$$

In Born approximation one arrives at the same expression for the conductivity Eq. (22) but the current-current correlation function is replaced by the much simpler expression

$$J^{\mathrm{Born}}(i\omega,i\Omega) = \frac{I_0^0(i\omega,i\Omega)}{1-\gamma^{\mathrm{Born}}(i\omega,i\Omega)I_0^0(i\omega,i\Omega)} \tag{23}$$

with the vertex function

$$\gamma^{\mathrm{Born}} = \frac{n_i}{4\pi v_f v_2}(V_1^2 - V_3^2). \tag{24}$$

So far we have focused on the effect of impurity scattering, which is appropriate for low temperatures and low frequencies. At higher temperatures, however, it is essential to take into account inelastic scattering processes as well, like, e.g., quasiparticle-quasiparticle scattering or scattering off spin fluctuations. These inelastic scattering processes are suppressed below $T_c$ due to the opening of the superconducting gap in the quasiparticle excitation spectrum and therefore the contribution of inelastic scattering increases rapidly when $T_c$ is approached from the low temperature side. A full treatment of inelastic scattering is beyond the scope of this paper. It has, however, been pointed out by Walker and Smith[27] that the contribution of quasiparticle-quasiparticle scattering to the transport lifetime is exponentially suppressed for low temperatures because only Umklapp scattering processes can decay the current and a finite excitation energy $\Delta_U$ is necessary to permit an Umklapp scattering process for a realistic Fermi surface. Thus, we include the effect of inelastic scattering by simply adding the inverse transport lifetime $\tau_{\mathrm{inel}}^{-1}(T)$ (see Fig. 3), which has been obtained by Duffy *et al.*[26] via extracting the Umklapp scattering processes from scattering of quasiparticles off spin fluctuations, to the imaginary part of the self-energy $\Sigma_0(\omega)$ in Eq. (11) or Eq. (15),

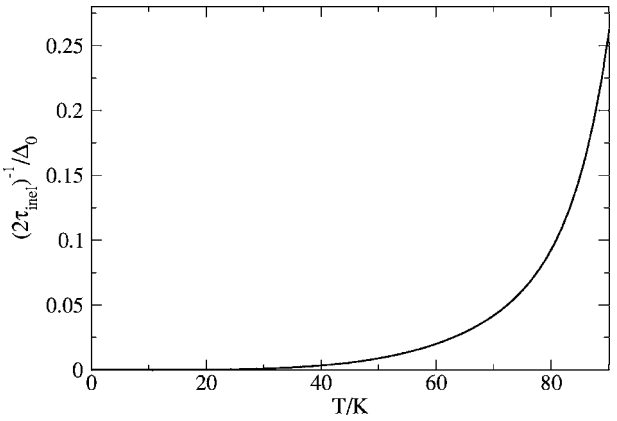


FIG. 3. Temperature dependence of the inelastic scattering rate $(2\tau_{\mathrm{inel}})^{-1}(T)$ used for the calculation of the microwave conductivity. This form has been obtained by Duffy *et al.* in Ref. 26 by extracting the Umklapp scattering processes from scattering of quasiparticles off spin fluctuations.

$$\Sigma_0^{\mathrm{tot}}(\omega,T) = \Sigma_0(\omega) - i[2\tau_{\mathrm{inel}}(T)]^{-1}. \tag{25}$$

Comparison of the inelastic scattering rate of Fig. 3 with the impurity self-energy of Fig. 2 shows that for small temperatures the contribution of inelastic scattering to the total self-energy is negligible, whereas for high temperatures the opposite is the case and the impurity self-energy becomes unimportant. Because the microwave conductivity is dominated by inelastic scattering at high temperatures we consider the small inaccuracies in the single-particle dispersion caused by the inappropriateness of the nodal approximation at high temperatures as irrelevant and display the microwave conductivity in the whole temperature range, where the temperature dependence of the superconducting gap is parametrized in the following way:[26]

$$\Delta_0(T) = \Delta_0 \tanh(\alpha\sqrt{T_c/T-1}) \tag{26}$$

using $\alpha=3.0$.

Note that our simplified treatment of $\tau_{\mathrm{inel}}^{-1}(T)$ completely neglects the frequency dependence of inelastic scattering and therefore limits our approach to small frequencies in the microwave regime, and prevents us from calculating the conductivity in the THz range.

## III. COMPARISON WITH EXPERIMENTAL SPECTRA OF YBCO

The microwave conductivity has been investigated in detail for pointlike scatterers within the self-consistent *T*-matrix approximation[2] and good agreement with the experimental data of YBCO has been found. The temperature dependence of the microwave conductivity for pointlike scatterers, see also Fig. 4, can be summarized in the following way. For zero temperature and zero frequency the conductivity approaches a universal value[8] $\sigma_0=e^2v_f/(\hbar\pi^2v_2)$ due to the fact that at zero temperature impurities give rise to a finite quasiparticle density of states while at the same time they reduce the quasiparticle lifetime. At low temperatures the conductivity rises with increasing $T$ due to an increase in the number of excited quasiparticles. The exact temperature dependence is determined by the density of states in a *d*-wave superconductor and the frequency dependence of the impurity scattering rate. Starting from the opposite side, i.e., decreasing the temperature below $T_c$, the conductivity also increases rapidly because inelastic scattering is suppressed below $T_c$ due to the opening of the superconducting gap in the quasiparticle excitation spectrum. This leads to the formation of a peak at intermediate temperatures, whose position is determined by the microwave frequency and the impurity scattering strength. This peak moves to higher temperatures and its amplitude decreases with increasing microwave frequency and impurity concentration.

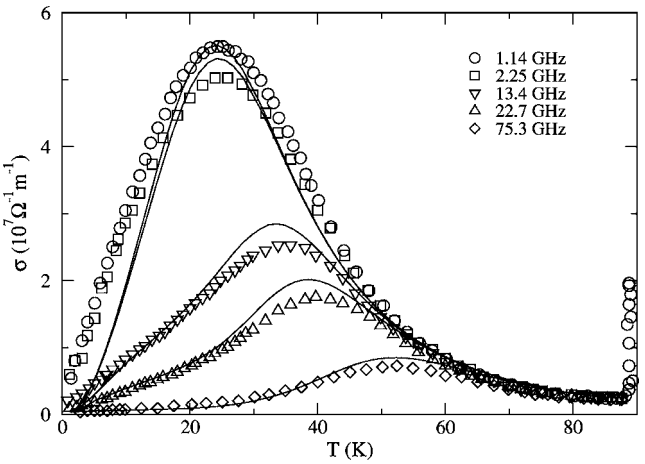


FIG. 4. Fit to the experimental spectra of YBCO (reproduced from Ref. 11) using pointlike strong scatterers with $V=100t$ and a concentration of $n_i=0.000\,035$. The magnitude of the conductivity has been scaled by a factor of 0.42, which corresponds to assuming a penetration depth of 1200 Å.

Our best fit to the experimental spectra of YBCO (Ref. 11) using pointlike strong scatterers is displayed in Fig. 4. Commonly used parameters for YBCO are $\Delta_0=400$ K for the gap maximum, $v_f/v_2=14$ for the anisotropy of the Dirac cone and $T_c=88.7$ K.[9,11] In order to compare our theoretical curves to the experimental data the value of the universal conductivity $\sigma_0=e^2v_f/(\hbar\pi^2v_2)$ must be translated into a three-dimensional conductivity which can be done via $\sigma_0^{3\mathrm{D}}=\sigma_0^{2\mathrm{D}}n_c$, where $n_c$ is the number of $CuO_2$ planes per unit length in the $c$ direction with $n_c=1/(5.9\ \text{Å})$ for YBCO. Because $\sigma\sim\lambda^{-3}$ the conductivity $\sigma$ is very sensitive to the value of the penetration depth $\lambda$, which has recently been claimed[29] as considerably smaller than previously published in the literature,[28] i.e., $\lambda=1030\pm80$ Å instead of $\lambda\simeq1550$ Å. This would increase the published values[11] of the microwave conductivity by a factor of 4. Indeed, it turns out that we obtain the best fit to the microwave conductivity of YBCO when we assume the absolute values of the conductivity to be roughly twice the previously published data,[11] which would correspond to a penetration depth of approximately 1200 Å. Therefore we allow ourselves the freedom to scale our calculated curves by roughly a factor of 1/2 when comparing to the experimental published values (exact scaling factor is stated in the figure captions).

As can be seen from Fig. 4 the assumption of pointlike scatterers can reproduce the temperature and frequency de-

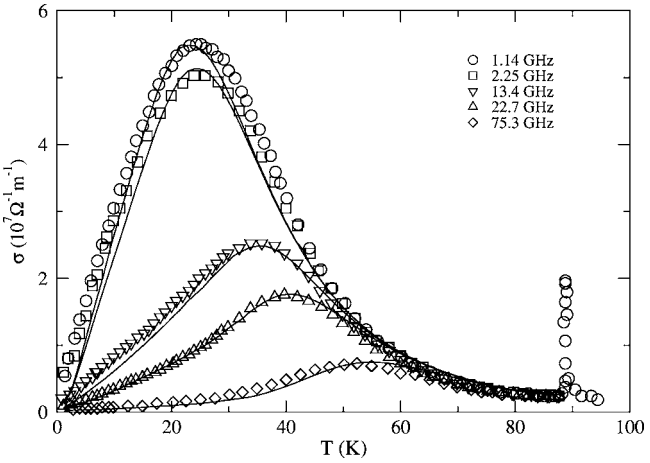


FIG. 5. Fit to the experimental spectra of YBCO (reproduced from Ref. 11) using slightly extended strong scatterers with $V_1=100t$, $V_2=85t$, $V_3=70t$ and a concentration of $n_i=0.000\,014$. The inelastic scattering rate has been slightly reduced by a factor of 0.8 with respect to Ref. 26 and the magnitude of the conductivity has been scaled by a factor of 0.34 which corresponds to assuming a penetration depth of 1100 Å.

pendence of the microwave conductivity of YBCO quite well (see Refs. 2–4). The largest discrepancy arises for low temperatures and low frequencies, where experimentally a nearly linear increase of the conductivity with temperature is found whereas the theory based on pointlike scatterers predicts a quadratic temperature dependence.[2] It has been suggested by Hettler and Hirschfeld[30] that the theoretical line shape becomes more linear at low temperatures when the suppression of the order parameter surrounding a strong pointlike scatterer is taken into account. This low temperature behavior has been attributed to the formation of a second resonance in the self-energy $\Sigma_0$ at low frequencies. It is intriguing to note that we find a similar resonance in the self-energy for slightly extended strong potential scatterers, see Fig. 2, and therefore it is interesting to investigate whether the presence of slightly extended potential scatterers can also explain the linear $T$ dependence of the microwave conductivity for low temperatures. Our best fit to the experimental spectra of YBCO using slightly extended potential scatterers is displayed in Fig. 5. Obviously the consideration of extended scatterers considerably improves the agreement with the experimental data at low temperatures.

Surprisingly, the concentration of extended scatterers used for the fit in Fig. 5 is even lower than the concentration of pointlike scatterers we have used for the fit in Fig. 4. Generally one would assume that due to the forward scattering character of extended impurities a larger concentration is necessary to obtain a similar scattering rate as for pointlike impurities. To gain more insight into this unexpected behavior we show in Fig. 6 the microwave conductivity for different spatial extensions of the scattering potential at two of the experimentally measured frequencies, i.e., 1.14 GHz and 13.4 GHz. Increasing the forward scattering character of the impurity potential slightly from $V_1=V_2=V_3=100t$ to $V_1=100t$, $V_2=85t$, and $V_3=70t$ essentially reduces the height of the peak in the conductivity at 1.14 GHz and makes the low

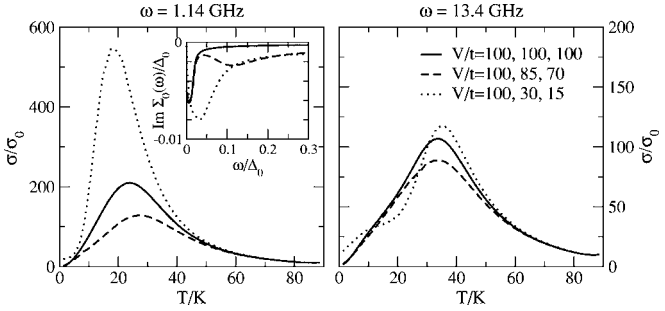


FIG. 6. Microwave conductivity for strong scatterers with varying degree of forward scattering. Impurity concentration, $n_i=0.000\,035$; maximum gap, $\Delta_0=0.29t$. Left panel, $\omega=1.14$ GHz; right panel, $\omega=13.4$ GHz. Inset, self-energy for the respective scattering potentials.

temperature increase more linear. For this small deviation from isotropic scattering, vertex corrections are small and the variation of the conductivity can be attributed to the formation of a second resonance in the self-energy at intermediate frequencies, see inset in Fig. 6 (see also discussion in Sec. II A). The nearly linear increase of the self-energy below the second resonance causes the more linear $T$ dependence of the conductivity at low temperatures. Only when the forward scattering character of the impurity potential is further enhanced, the vertex corrections begin to outweigh the growing self-energy and the conductivity rises above the values obtained for isotropic scattering. For these more extended scattering potentials the second resonance in the self-energy moves to lower frequencies until it merges with first resonance. For the larger microwave frequency of 13.4 GHz, see right-hand panel of Fig. 6, the anisotropy of the impurity potential has less effect. This implies that for slightly extended impurity potentials as considered for YBCO in Fig. 5 the frequency dependence becomes much weaker and therefore a smaller concentration than in the case of pointlike impurities is necessary to reproduce the experimentally observed frequency dependence. We emphasize that this analysis, while establishing the relevance of extended nature of dopant impurities to this problem, cannot rule out other explanations[30–32] for the quasilinear in $T$ behavior observed at low frequencies.

## IV. COMPARISON WITH EXPERIMENTAL SPECTRA OF BSCCO

In this section we want to explore what can be learned about the type of disorder contained in the BSCCO compounds by analyzing its microwave conductivity which was measured by Lee *et al.*[12] The temperature and frequency dependence of the microwave conductivity in BSCCO (see symbols in Fig. 7) is quite different than in YBCO. The absolute value of the microwave conductivity is smaller by almost a factor of 10 indicating that BSCCO is a dirtier compound than YBCO. This agrees well with the observation that the conductivity of BSCCO changes noticeably only in the THz regime,[13] i.e., at much higher frequencies than in YBCO. The characteristic peak in the microwave conductiv-

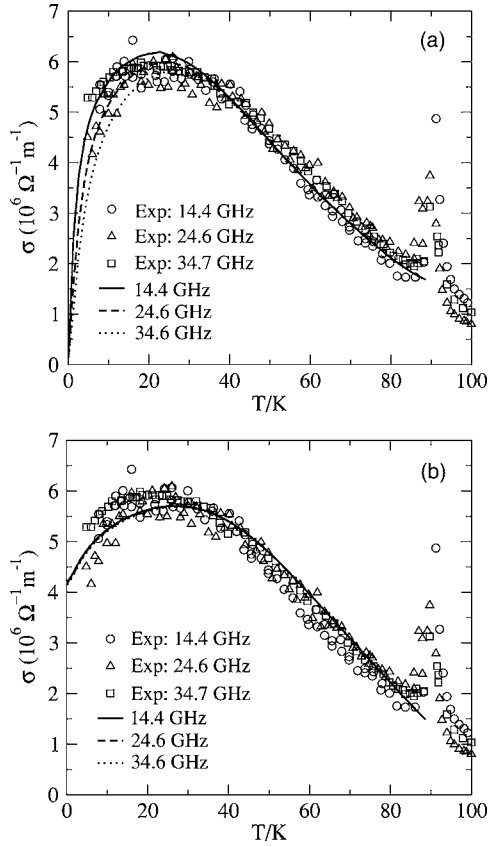


FIG. 7. Fit to the experimental microwave conductivity of BSCCO (reproduced from Ref. 12) using weak scatterers, (a) pointlike scatterers with $V/t=1$ and $n=0.049$, (b) weak extended scatterers with $V_1/t=2$, $V_2/t=0.8$, $V_3/t=0.4$, and $n=0.145$. [The inelastic scattering rate has been increased by a factor of 2.6 in (a) and 3 in (b) with respect to Ref. 26.]

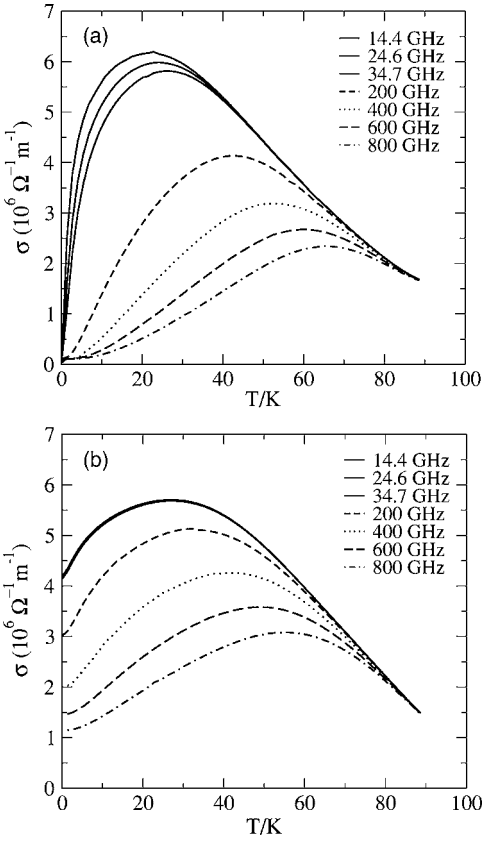


FIG. 8. Higher frequency conductivity for the disorder models of Fig. 7, (a) pointlike scatterers with $V/t=1$ and $n=0.049$, (b) weak extended scatterers with $V_1/t=2$, $V_2/t=0.8$, $V_3/t=0.4$, and $n=0.145$.

ity, however, occurs at lower temperatures than in the cleaner system YBCO contrary to predictions for strong pointlike scatterers.[2] Furthermore this peak is much less pronounced and resembles more a plateau, suggestive of the weak scattering limit.[2] Finally, the conductivity does not apparently approach the universal value $\sigma_0$ for the lowest temperatures and frequencies measured. This might indicate the presence of extended scatterers, which enhance the zero-temperature and zero-frequency limit of the conductivity as has been pointed out by Durst and Lee.[22]

In order to check the applicability of these scenarios for BSCCO we compare in Fig. 7 respective fits to the microwave conductivity using (i) only pointlike weak scatterers [Fig. 7(a)] and (ii) only extended weak scatterers [Fig. 7(b)]. For the inelastic scattering rate $\tau_{\mathrm{inel}}^{-1}(T)$ we assume the same temperature dependence as for YBCO (Ref. 26) but we allow for a different prefactor in order to account for discrepancies between YBCO and BSCCO (the exact prefactor is stated in the figure captions). Obviously both disorder models (i) and (ii) result in very good fits of the experimental microwave conductivity of BSCCO. The main difference is that the conductivity for isotropic scatterers approaches the universal value $\sigma_0$ for $T\rightarrow 0$ whereas the conductivity for extended scatterers [Fig. 7(b)] with the potential parameters $V_1/t=2$, $V_2/t=0.8$, and $V_3/t=0.4$ approaches an enhanced value. Unfortunately, it is not possible to distinguish between these two different scenarios from the microwave conductivity alone, because there is no experimental data available below $T=5$ K.

Further insight could be gained by comparing the frequency dependence of these two models. Impurity scattering alone would predict a different frequency dependence for isotropic and extended scatterers, as illustrated in Fig. 8. Whereas the magnitude of the conductivity remains rather large at low temperatures in the case of extended scatterers even for high frequencies, it almost vanishes in the case of pointlike impurities. Due to the large impurity concentration this frequency dependence is most pronounced in the THz regime as observed experimentally.[13] In the THz range, however, a more refined treatment of inelastic scattering than Eq. (25) is indispensable, including, e.g., its frequency dependence and possibly an explicit evaluation of inelastic vertex corrections. Thus, the THz data present not only a probe of elastic impurity scattering but also of inelastic scattering processes and are therefore not directly suitable to distinguish between pointlike and extended impurities.

The only way we can proceed now is try to exclude one of the two models indirectly via analyzing an additional observable. Thus we will argue in the following that disorder model (i) containing 4.9% weak isotropic scatterers with a scattering strength of $V=1t$ would yield an unrealistically large

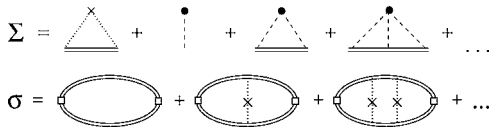

FIG. 9. Diagrams for the self-energy $\Sigma$ and microwave conductivity $\sigma$ considered in the realistic disorder model for BSCCO. Circles denote the pointlike strong impurities, which are treated in the $T$-matrix approximation. Crosses denote the weak extended scatterers, which are treated in the Born approximation. Only the extended, i.e., only the weak scatterers contribute to the vertex corrections.

normal state scattering rate. Assuming a normal state density of states of $1/8t$ yields a normal state scattering rate of $\tau^{-1} \approx 0.6T_c$ for $t=120$ meV. According to Abrikosov-Gorkov's scaling law this would reduce $T_c$ by 25%, which we consider as an unreasonably large suppression because $T_c \approx 93$ K in the samples used for microwave conductivity in Ref. 12, which is close to the highest values of $T_c$ measured for the BSCCO compounds. Extended impurities, on the other hand, act mainly as small angle scatterers and affect $T_c$ much less than isotropic scatterers.[34,35] This allows us to assess model (i), which consists only of weak pointlike scatterers, as very unlikely and to conclude that at least a large fraction of the disorder in the BSCCO compounds should be attributed to extended scatterers. This could be confirmed by microwave experiments on crystals at lower $T$.

So far we have focused on the effect of weak scatterers which we attribute to the out-of plane disorder introduced by doping. Defects within the $CuO_2$ planes, on the other hand, are generally considered to act as strong pointlike scatterers. These strong scattering defects have been observed in STM experiments[33] on BSCCO compounds and are often assumed to be the main source of disorder in the YBCO compounds although their concentration is very low. We therefore now address the question of whether our model for the microwave conductivity in BSCCO is compatible with an additional small concentration of strong pointlike impurities, which are most likely also present in the compound used for measurements of the microwave conductivity of BSCCO in Ref. 12.

We incorporate this realistic disorder model, which consists of weak extended and strong pointlike scatterers, by calculating the diagrams depicted in Fig. 9. The weak extended scatterers are treated in Born approximation and the strong pointlike impurities in $T$-matrix approximation. Because vertex corrections vanish for pointlike scatterers, only the weak extended scatterers contribute and the vertex corrections can be calculated in Born approximation. Thus, the microwave conductivity $\sigma(\Omega)$ is still given by Eq. (22) with the bubble $J^{\mathrm{Born}}(\omega,\Omega)$ as in Eq. (23) and the vertex function $\gamma^{\mathrm{Born}}$ given in Eq. (24). Only the self-energy $\Sigma_0$ must be calculated self-consistently as the sum of Eq. (12), Eq. (15), and the inelastic scattering rate

$$\Sigma_0(\omega,T) = \frac{n_s 4g_0(\omega)V_s^2}{[1-4g_3(\omega)V_s]^2 - [4g_0(\omega)V_s]^2} - n_w(V_1^2+2V_2^2+V_3^2)g_0(\omega) - i[2\tau_{\mathrm{inel}}(T)]^{-1}. \tag{27}$$

Here, $n_s$ is the concentration of strong pointlike impurities

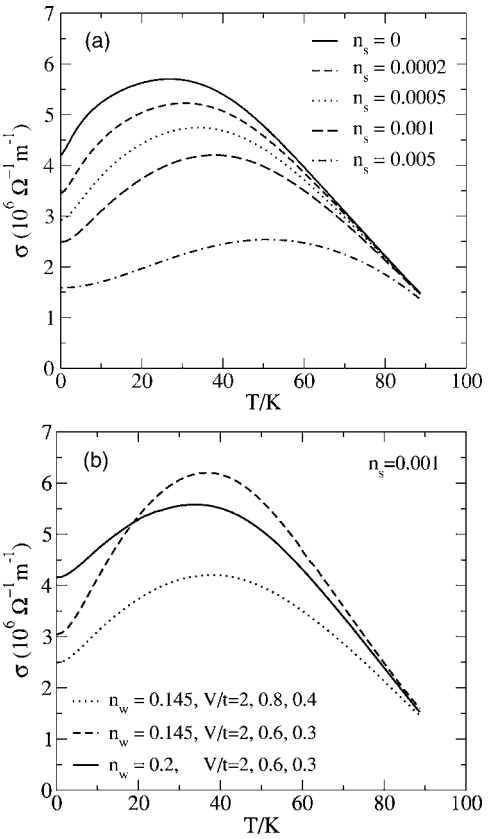


FIG. 10. Effect of adding strong pointlike scatterers for the microwave conductivity at 14.4 GHz. (a) Weak extended scatterers with parameters of Fig. 7(b), i.e., $n_w=0.145$ and $V_1/t=2$, $V_2/t=0.8$, $V_3/t=0.4$, and additional strong pointlike scatterers with $V/t=100$ and different concentrations $n_s$. (b) Fixed concentration $n_s=0.001$ of strong pointlike impurities for varying concentration and forward scattering potential of the weak scatterers.

with a scattering potential $V_s$, $n_w$ is the concentration of weak extended scatterers characterized by the potential parameters $V_1,V_2,V_3$, and $g_0(\omega),g_3(\omega)$ are the Nambu components of the momentum integrated single particle Green's function as defined in Eq. (8). Note that "strong impurity" implies a potential $V_s$ chosen so that the 1-impurity resonance lies essentially at the Fermi level. For our purposes, this means any value $V_s \gtrsim 20t$ could be chosen, and changing $V_s$ does not change the results for the conductivity in this limit.

The effect of adding a small concentration of strong pointlike scatterers to the extended weak scatterers used in Fig. 7(b) is illustrated in Fig. 10. Additional strong pointlike scatterers mainly reduce the conductivity as can be seen in Fig. 10(a). In order to raise the conductivity to its previous values the forward scattering character of the weak impurities must therefore be enhanced. On the other hand, this increases the difference between the zero-temperature value and the maximum value of the conductivity [see dashed line in Fig. 10(b)] and necessitates a larger concentration of weak extended scatterers. Finally the line shape of the conductivity [solid line in Fig. 10(b)] looks similar to the one without strong pointlike impurities but it is flatter at low temperatures than before. This poses an upper limit for the concentration of

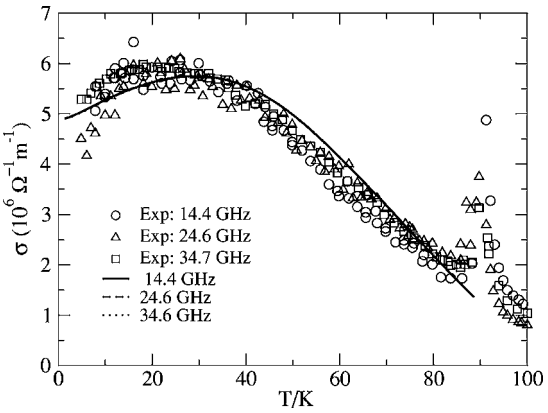


FIG. 11. Fit to the experimental microwave conductivity of BSCCO (reproduced from Ref. 12) using $n_w=0.1$ weak extended scatterers with $V_1/t=3$, $V_2/t=0.9$, $V_3/t=0.5$, and $n_s=0.0005$ strong pointlike scatterers with $V_s/t=100$. (The inelastic scattering rate has been increased by a factor of 3.4 with respect to Ref. 26.)

strong scatterers compatible with the experimental microwave conductivity of BSCCO.

A fit to the experimental microwave conductivity of BSCCO containing 0.05% pointlike strong scatterers and 10% weak extended scatterers is shown in Fig. 11. This is about the largest concentration of pointlike strong scatterers still compatible with our fit to the microwave conductivity. This concentration is smaller than the 0.2% observed in STM experiments[33] on BSCCO but it is very plausible that the number of in-plane defects varies between bulk and surface.

## V. CONCLUSIONS

In summary, we have investigated the influence of extended scatterers on the microwave conductivity of *d*-wave superconductors by extending the approach of Durst and Lee,[22] which is based on a nodal approximation for the quasiparticle spectrum and the impurity potential, to finite temperatures and frequencies. Self-energy and vertex corrections are calculated within the self-consistent *T*-matrix approximation.

The effect of extended scatterers on the temperature and frequency dependence of the microwave conductivity can be summarized as follows: for a small concentration of slightly extended strong scatterers a second resonance forms in the self-energy at intermediate frequencies similar to treatments which consider the suppression of the order parameter surrounding a strong pointlike impurity.[30] This results in a more linear temperature dependence of the conductivity at low temperatures and therefore improves the agreement with experimental spectra of YBCO at low temperatures. For more extended scatterers the vertex corrections begin to dominate over the self-energy and the magnitude of the conductivity increases.

The microwave conductivity of BSCCO is very different compared to YBCO and cannot be understood even qualitatively in terms of only strong scattering pointlike impurities. We find that a large concentration of weak extended scatterers is necessary to explain the observed temperature and frequency dependence of the microwave conductivity in BSCCO, where (i) the impurity concentration must be large to explain the small magnitude of the conductivity and the negligible frequency dependence in the microwave range, (ii) the scattering strength must be small to account for the plateaulike line shape of the conductivity at small temperatures, and (iii) the range of the scattering potential must be spatially extended in order to keep the $T_c$ suppression reasonably small.[34] Finally, we have shown that adding a small concentration of pointlike strong scatterers, which have been observed in STM experiments,[33] to the weak extended scattering potential, which we attribute to the out-of-plane disorder introduced by doping, is still compatible with the microwave conductivity of BSCCO. Although it would be necessary to refine our treatment of inelastic scattering by accounting for its frequency dependence and its contribution to vertex corrections in order to address the conductivity in the THz range,[13] it is interesting to note that elastic scattering alone would predict a very different frequency dependence for pointlike and extended scatterers.

## ACKNOWLEDGMENTS

This work was supported by a Feodor-Lynen Fellowship from the A. v. Humboldt Foundation (T.S.N.) and ONR Grant No. N00014-04-0060 (P.J.H.). The authors are grateful to D. A. Bonn, R. Harris, I. Bosovic, L.-Y. Zhu, D. J. Scalapino, and P. Wölfle for stimulating conversations.

[1] D. A. Bonn, R. Liang, T. M. Riseman, D. J. Baar, D. C. Morgan, K. Zhang, P. Dosanjh, T. L. Duty, A. MacFarlane, G. D. Morris, J. H. Brewer, W. N. Hardy, C. Kallin, and A. J. Berlinsky, Phys. Rev. B **47**, 11314 (1993).

[2] P. J. Hirschfeld, W. O. Putikka, and D. J. Scalapino, Phys. Rev. Lett. **71**, 3705 (1993); Phys. Rev. B **50**, 10250 (1994).

[3] C. T. Rieck, K. Scharnberg, and J. Ruvalds, Phys. Rev. B **60**, 12432 (1999).

[4] E. Schachinger and J. P. Carbotte, Phys. Rev. B **57**, 7970 (1998); **65**, 064514 (2002).

[5] D. A. Bonn, P. Dosanjh, R. Liang, and W. N. Hardy, Phys. Rev. Lett. **68**, 2390 (1992).

[6] M. C. Nuss, P. M. Mankiewich, M. L. O'Malley, E. H. Westerwick, and P. B. Littlewood, Phys. Rev. Lett. **66**, 3305 (1991).

[7] D. B. Romero, C. D. Porter, D. B. Tanner, L. Forro, D. Mandrus, L. Mihaly, G. L. Carr, and G. P. Williams, Phys. Rev. Lett. **68**, 1590 (1992).

[8] P. A. Lee, Phys. Rev. Lett. **71**, 1887 (1993).

[9] M. Chiao, R. W. Hill, Ch. Lupien, B. Popic, R. Gagnon, and L. Taillefer, Phys. Rev. Lett. **82**, 2943 (1999); K. Behnia, S. Belin, H. Aubin, F. Rullier-Albenque, S. Ooi, T. Tamegai, A. Deluzet, and P. Batail, J. Low Temp. Phys. **117**, 1089 (1999).

[10] J. Mesot, M. R. Norman, H. Ding, M. Randeria, J. C. Campuzano, A. Paramekanti, H. M. Fretwell, A. Kaminski, T. Takeuchi, T. Yokoya, T. Sato, T. Takahashi, T. Mochiku, and K. Kadowaki, Phys. Rev. Lett. **83**, 840 (1999).
[11] A. Hosseini, R. Harris, Saeid Kamal, P. Dosanjh, J. Preston, Ruixing Liang, W. N. Hardy, and D. A. Bonn, Phys. Rev. B **60**, 1349 (1999).
[12] Shih-Fu Lee, D. C. Morgan, R. J. Ormeno, D. Broun, R. A. Doyle, J. R. Waldram, and K. Kadowaki, Phys. Rev. Lett. **77**, 735 (1996).
[13] J. Corson, J. Orenstein, S. Oh, J. O'Donnell, and J. N. Eckstein, Phys. Rev. Lett. **85**, 2569 (2000).
[14] J. Orenstein, Physica C **390**, 243 (2003).
[15] H. Eisaki, N. Kaneko, D. L. Feng, A. Damascelli, P. K. Mang, K. M. Shen, Z.-X. Shen, and M. Greven, Phys. Rev. B **69**, 064512 (2004).
[16] E. Abrahams and C. M. Varma, Proc. Natl. Acad. Sci. U.S.A. **97**, 5714 (2000).
[17] Lingyin Zhu, W. A. Atkinson, and P. J. Hirschfeld, Phys. Rev. B **69**, 060503(R) (2004).
[18] C. Howald, P. Fournier, and A. Kapitulnik, Phys. Rev. B **64**, 100504(R) (2001).
[19] J. E. Hoffmann, K. McElroy, D.-H. Lee, K. M. Lang, H. Eisaki, S. Uchida, and J. C. Davis, Science **297**, 1148 (2002).
[20] K. McElroy, R. W. Simmonds, J. E. Hoffman, D.-H. Lee, J. Orenstein, H. Eisaki, S. Uchida, and J. C. Davis, Nature (London) **422**, 592 (2003).
[21] L. Zhu, P. J. Hirschfeld, and D. J. Scalapino, Phys. Rev. B **70**, 214503 (2004).
[22] A. C. Durst and P. A. Lee, Phys. Rev. B **62**, 1270 (2000).
[23] I. Adagideli, D. E. Sheehy, and P. M. Goldbart, Phys. Rev. B **66**, 140512(R) (2002).
[24] D. E. Sheehy, Phys. Rev. B **68**, 054529 (2003).
[25] P. J. Hirschfeld, P. Wölfle, and D. Einzel, Phys. Rev. B **37**, 83 (1988).
[26] D. Duffy, P. J. Hirschfeld, and D. J. Scalapino, Phys. Rev. B **64**, 224522 (2001).
[27] M. B. Walker and M. F. Smith, Phys. Rev. B **61**, 11285 (2000).
[28] J. L. Tallon, C. Bernhard, U. Binninger, A. Hofer, G. V. M. Williams, E. J. Ansaldo, J. I. Budnick, and Ch. Niedermayer, Phys. Rev. Lett. **74**, 1008 (1995).
[29] T. Pereg-Barnea, P. J. Turner, R. Harris, G. K. Mullins, J. S. Bobowski, M. Raudsepp, R. Liang, D. A. Bonn, and W. N. Hardy, Phys. Rev. B **69**, 184513 (2004).
[30] M. H. Hettler and P. J. Hirschfeld, Phys. Rev. B **59**, 9606 (1999); **61**, 11313 (2000).
[31] A. C. Durst and P. A. Lee, Phys. Rev. B **65**, 094501 (2002).
[32] S. Hensen, G. Müller, C. T. Rieck, and K. Scharnberg, Phys. Rev. B **56**, 6237 (1997).
[33] E. W. Hudson, S. H. Pan, A. K. Gupta, K.-W. Ng, and J. C. Davis, Science **285**, 88 (1999); E. W. Hudson *et al.*, Physica B **329**, 1365 (2003).
[34] Hae-Young Kee, Phys. Rev. B **64**, 012506 (2001).
[35] G. Haran and A. D. S. Nagi, Phys. Rev. B **54**, 15463 (1996); **58**, 12441 (1998); M. L. Kulic and O. V. Dolgov, *ibid.* **60**, 13062 (1999).